



Republic of Iraq  
Ministry of Higher  
Education  
and Scientific Research  
University of Diyala  
College of Science  
Department of Physics



# **Enhancement of Gas Sensing Properties of Metal Oxides Thin Films by Embedding of Noble Metals Nanoparticles**

A thesis

Submitted to the Council of the College of Science  
University of Diyala in Partial Fulfillment of Requirements for  
the Degree of Doctor of Philosophy in Physics

By

ASAAD AHMED KAMIL

Supervised By

Prof. Dr.  
Nabeel Ali Bakr

Prof. Dr.  
Tahseen Hussien Mubarak

2022 A.D

1444 A.H

بِسْمِ اللَّهِ الرَّحْمَنِ الرَّحِيمِ

نَرْفَعُ دَرَجَاتٍ مِّنْ نَّشَاءٍ وَفَوْقَ كُلِّ ذِي  
عِلْمٍ عِلْمٍ

صدق الله العظيم

سورة يوسف الآية ٧٦

# Dedication

To .....

The lights of my life soul  
Father & Mother

The lights of my eyes my wife, my son Mustafa, my  
daughters, Tabark and Yusur

To My Lovely Family  
My Brother and My Sisters.

To All My Friends.

All faithful hearts who helped me  
in the journey of my life.

Asaad

## **Acknowledgement**

First and foremost, I would like to thank Almighty Allah for giving me the strength, knowledge, ability and opportunity to undertake, persevere and complete this research. Without his blessings, this achievement would not have been possible. I also thank our prophet Muhammad (peace and blessings of Allah be upon him) who invites us to science and work. I would like to express my sincere appreciation and deep gratitude to my supervisors, Prof. Dr. Nabeel Ali Bakr and Prof. Dr. Tahseen Hussien Mubarak for suggesting the topic of this thesis, intuitive insight, constant encouragement, unconditional support and unlimited cooperation extended to me during the course of my research work.

I would like to express my profound gratitude to Prof. Dr. Sabah A. Salman, Prof. Dr. Ziad T. Khodair, Assist. Prof. Dr. Jasim M. Mansoor, Assist. Prof. Dr. Mohammed Hameed, Assist. Prof. Dr. Jassim M. Khalel, Prof. Dr. Issam M. Ibrahim (Baghdad University, College of Science), Assist. Prof. Dr. Issam H. Hameed, Prof. Firas M. Hadi and Assist. Prof. Faisal G. Hammody for their kind cooperation and constant support. I am highly indebted to encouragement throughout my study.

Special thanks are extended to the University of Diyala, College of Science, Department of Physics, the head of the department Assist. Prof. Dr. Amar A. Habeeb, and all the Staff of the College of Science and Department of Physics for their assistance.

I would like to express my profound gratitude to the members of the College of Science council and all colleagues of College of Science.

I am grateful to my colleagues in laboratory at Physics Dept. College of Science, University of Diyala, (Karrar, Ali Menhal, Saif, Laith, Hala , Israa Mohammed and Haidar). I would also like to thank Dr. Fuaad (Baghdad University, College of Science), Dr. Adnan Abo Ayman, Dr. Mustafa Zaid, Marwa Jwameer for their help in making measurements.

## **Published and Accepted Research Articles**

1. A. A. Kamil, N. A. Bakr, T. H. Mubarak and J. Al-Zanganawee " Synthesis and study of the optical and structural properties of Au and Ag nanoparticles by pulsed laser ablation (PLAL) technique " Digest Journal of Nanomaterials and Biostructures Vol. 16, No. 4, October-December 2021, p. 1219-1226.
2. Asaad A. Kamil, Nabeel A. Bakr, Tahseen H. Mubarak and J. Al-Zanganawee "Effect of Au and Ag Nanoparticles Addition on the morphological structural and Optical Properties of ZnO Thin Films Deposited by Sol- Gel Method" Journal of Ovonic Research Vol. 18, No. 3, May - June 2022, p. 431 - 442

## Supervisor Certification

---

We certify that this thesis entitled "**Enhancement of Gas Sensing Properties of Metal Oxides Thin Films by Embedding of Noble Metals Nanoparticles**" submitted by (**ASAAD AHMED KAMIL**) was prepared under our supervision at the Department of Physics, College of Science, University of Diyala in a partial fulfillment of the requirements needed to award the Degree of Doctor of Philosophy (Ph. D.) in Science of Physics.

Signature:

Name: Dr. Nabeel A. Bakr

Title: Professor

Address: Dep.of Physics, College of  
Science, University of Diyala

Date: / / 2022

Signature:

Name: Dr. Tahseen H. Mubarak

Title: Professor

Address: Dep.of Physics, College of  
Science, University of Diyala

Date: / / 2022

### **Head of the Physics Department**

In view of the available recommendations, I forward this thesis for debate by the examination committee.

Signature:

Name: Dr. Ammar A. Habeeb

Title: Assistant Professor

Address: Head of the Physics Department, College of Science, University of Diyala

Date: / / 2022

## **Linguistic Amendment**

I certify that the thesis entitled "**Enhancement of Gas Sensing Properties of Metal Oxides Thin Films by Embedding of Noble Metals Nanoparticles** " presented by (**ASAAD AHMED KAMIL**) has been corrected linguistically, therefore, it is suitable for debate by examining committee.

Signature:

Name: Dr. Esam H. Hameed

Title: Assistant Professor

Address: College of Science, University of Diyala

Date:    /    / 2022

## **Scientific Amendment**

I certify that the thesis entitled "**Enhancement of Gas Sensing Properties of Metal Oxides Thin Films by Embedding of Noble Metals Nanoparticles**" presented by (**ASAAD AHMED KAMIL**) has been evaluated scientifically, therefore, it is suitable for debate by examining committee.

Signature:

Name: Dr. Bahjat B. Kazem

Title: Professor

Address: Dep. of Physics, College of Science, University of Al Mustansiriya

Date:     /     /2022



## **Scientific Amendment**

I certify that the thesis entitled "**Enhancement of Gas Sensing Properties of Metal Oxides Thin Films by Embedding of Noble Metals Nanoparticles**" presented by (**ASAAD AHMED KAMIL**) has been evaluated scientifically, therefore, it is suitable for debate by examining committee.

Signature:

Name: Dr. Bushra K. Hassoon

Title: Professor

Address: Dep. of Physics, College of Education for pure Science  
(Ibn Al- Haitham) , University of Baghdad

Date:     /     /2022

## Examination Committee Certificate

---

We certify that we have read this thesis entitled "**Enhancement of Gas Sensing Properties of Metal Oxides Thin Films by Embedding of Noble Metals Nanoparticles**" presented by (ASAAD AHMED KAMIL) and as an examine committee, we examined the student on its contents, and in what is related to it, and that in our opinion it meets the standard of a thesis for the **Degree of Doctor of Philosophy (Ph.D.) in Science of physics.**

Signature:

Name: Dr.Nadir F. Habubi

Title: Professor

Date: / /2022

(Chairman)

Signature:

Name:Dr.Sabah A. Salman

Title: Professor

Date: / /2022

(Member)

Signature:

Name:Dr.Abdul Hadi K. Judran

Title: Professor

Date: / /2022

(Member)

Signature:

Name: Dr. Zaid T. Khodair

Title: Professor

Date: / /2022

(Member)

Signature:

Name:Dr.Ammar A. Habeeb

Title: Professor

Date: / /2022

(Member)

Signature:

Name: Dr. Nabeel A. Bakr

Title: Professor

Date: / /2022

(Supervisor)

Signature:

Name:Dr.Tahseen H. Mubarak

Title: Professor

Date: / /2022

(Supervisor)

**Approved by the Council of the College of Science:**

Signature:

Name: Dr. Tahseen H. Mubarak

Title: Professor

Address: Dean of College of the Science, University of Diyala

Date: / /2022

## **Abstract**

In this study, Au and Ag NPs were synthesized in distilled water by Pulsed Laser Ablation in Liquid (PLAL) technique using Q-switched (Nd:YAG) pulsed laser with laser parameters (520 mJ laser energy, 1064 nm wavelength, and 1Hz frequency). The effect of six different laser pulses (150, 250, 350, 450, 550, and 650) on the properties of these NPs were investigated systematically. ZnO and SnO<sub>2</sub> thin films were deposited on glass substrates by sol-gel spin-coating method. Volumetric ratios of ZnO and SnO<sub>2</sub> solutions with Au and Ag colloidal solution (3:2 and 4:1) were used to prepare ZnO and SnO<sub>2</sub> thin films embedded with Au and Ag NPs, and the morphological, structural, optical and Hall Effect properties of all the films were investigated. TEM micrographs of Au and Ag NPs shows that all samples were spherical in shape. The XRD patterns of the Au and Ag NPs exhibited the pure cubic crystalline structure at all the pulses used. The XRD patterns of Ag NPs also showed the formation of another cubic crystal structure attributed to AgO. FESEM images of the films exhibited spherical particles and randomly scattered spherical particles having irregular sizes for ZnO+Au (3:2) and ZnO+Au (4:1), respectively and showing cauliflower like shapes with irregular size-distribution for ZnO+Ag (3:2) and randomly scattered cauliflower particles having irregular shapes and sizes for ZnO+Ag (4:1). The images of SnO<sub>2</sub>+Au (3:2) and SnO<sub>2</sub>+Au (4:1) display that most of the particles obtained have spherical shapes and are agglomerated due to their small sizes. The XRD patterns of all ZnO thin films showed that the diffraction peaks belong to the hexagonal phase with a wurtzite structure, while the XRD patterns of all SnO<sub>2</sub> thin films exhibited diffraction peaks which belong to the tetragonal rutile crystal. Raman spectroscopy studies show that the peaks of ZnO and SnO<sub>2</sub> thin films embedded with Au and Ag NPs at volume ratio (3:2) are Raman-active peaks consistent vibration modes. It can be notice four typical peaks at Raman shift of 312, 453, 562 and 790

$\text{cm}^{-1}$  for (ZnO +Au) thin film and observed three peaks at 420, 560 and 825  $\text{cm}^{-1}$  are the transverse optical (TO), longitudinal optical (LO) polar branches, respectively for (ZnO +Ag) thin film. Also, show two of the four fundamental Raman-active peaks at 751 and 807  $\text{cm}^{-1}$  for (SnO<sub>2</sub>+Au) thin film and five peaks at 237, 421, 473, 561 and 749  $\text{cm}^{-1}$  for (SnO<sub>2</sub>+Ag) thin film. The absorbance values of the films decrease with the increase of wavelength, it is increase as the molarity of ZnO and SnO<sub>2</sub> increases. It can be notice that the absorbance increase with the volumetric ratios of ZnO and SnO<sub>2</sub> thin films embedded with Au and Ag NPs increasing. The absorption coefficient of ZnO and SnO<sub>2</sub> thin films embedded with Au and Ag NPs at different volume ratios (3:2 and 4:1) increase gradually with the increase in the energy of the incident photons until it reaches the value of  $10^4 \text{ cm}^{-1}$ , the values of the absorption coefficient greater than  $10^4 \text{ cm}^{-1}$  indicate the possibility of allowed direct electronic transitions. The value of optical energy gap of ZnO and SnO<sub>2</sub> thin films embedded with Au and Ag NPs at different volume ratios (3:2 and 4:1) obtained are (3.92, 3.90, 3.99 and 3.97 eV) and (3.56, 3.58, 3.80 and 3.85 eV), respectively. Hall Effect measurements of ZnO thin films embedded with Au and Ag NPs show that the conductivity increases as carrier concentration increases. It can be notice that the resistivity decreases as carrier concentration increases for AuNPs embedded with ZnO, while it is increases for AgNPs embedded with ZnO. The measurements of SnO<sub>2</sub> thin films embedded with Au and Ag NPs show the conductivity increases as carrier concentration decreases, and the resistivity is decreases at a high amount of Au and Ag. Gas sensor results show that the maximum sensitivity of (SnO<sub>2</sub>+Au) sensor to 60 ppm of NO<sub>2</sub> gas is greater than (ZnO+Ag) sensor. The results show the sensitivity increase as the operating temperature and as the concentration of the NO<sub>2</sub> and NH<sub>3</sub> gas increases. Also can be notice that the response and recovery times decrease as the operating temperature increases.

## List of Contents

No.	Subjects	Page No.
<b>Chapter One: Introduction</b>		
1.1	Introduction	1
1.2	Thin Films Deposition Technique	1
1.3	Metal Oxides	2
1.3.1	Tin Oxide (SnO <sub>2</sub> )	3
1.3.2	Zinc Oxide (ZnO)	5
1.4	Nanotechnology	7
1.5	Nanoparticles Synthesis Methods	7
1.5.1	Top-down method	7
1.5.2	Bottom-up method	8
1.6	Definition of Nanoparticles	8
1.6.1	Noble Metal Nanoparticles	8
1.6.2	Nanoparticles Preparation techniques	9
1.7	Pulsed Laser Ablation (PLA) Method	10
1.7.1	Pulse Laser Ablation in Liquids (PLAL)	12
1.8	Spin coating techniques	14
1.9	The sol-gel method	15
1.10	Previous Studies	16
1.11	Aims of the Work	28
<b>Chapter Two: Theoretical Part</b>		
2.1	Introduction	29
2.2	Semiconductors Materials	29
2.3	Classification of Semiconductors	30
2.3.1	Crystalline Semiconductors	30
2.3.2	Amorphous Semiconductors	31
2.4	Electronic Transitions	32
2.4.1	Direct Transitions	32
2.4.2	Indirect Transitions	32
2.5	Optical Constants	33
2.5.1	Absorption Coefficient	34
2.5.2	Ultra violet-visible spectroscopy	34
2.6	Fundamental Absorption Edge	35
2.6.1	High Absorption Region	35
2.6.2	Exponential Region	36
2.6.3	Low Absorption Region	36

2.7	Structural Parameters	37
2.7.1	X –ray diffraction	37
2.7.2	Crystallite Size ( $D_{av}$ )	38
2.7.3	Lattice constants	40
2.7.4	Dislocations Density	40
2.7.5	Microstrain ( $\epsilon$ )	40
2.8	Raman Spectroscopy	41
2.9	Electrical Properties of Semiconductors	41
2.9.1	D.C Electrical Conductivity ( $\sigma_{D.C.}$ )	42
2.9.2	Hall Effect	43
2.10	Gas Sensors	44
2.10.1	Gas Sensor Applications	45
2.10.2	Mechanism of Gas Sensing	46
2.10.3	Metal oxides (MOS) gas sensors	47
2.11	Gas sensing parameters	48
2.11.1	Sensor resistance to gas concentration characteristics	48
2.11.2	Sensitivity ( $S_g$ )	48
2.11.3	Response time	49
2.11.4	Recovery Time	49
2.11.5	Operating temperature	50
2.11.6	Selectivity	50
2.11.7	Stability	50
2.12	Methods to improve gas sensing response	50
2.12.1	Doping and catalysts	50
2.12.2	Grain size effects	51
2.12.3	Thickness dependence	51
2.12.4	Temperature modulation	52
<b>Chapter Three: Experimental Part</b>		
3.1	Introduction	53
3.2	Chemicals and Raw Materials	53
3.3	Substrate Cleaning Steps	55
3.4	Thin Film Preparation	55
3.4.1	ZnO Thin Film Preparation	56
3.4.2	SnO <sub>2</sub> Thin Films Preparation	56
3.5	Spin Coating System	58
3.6	Synthesis of gold and silver NPs by PLAL	59
3.6.1	Thin Film Preparation Au and Ag nanoparticles	60
3.7	ZnO and SnO <sub>2</sub> Embedded with Au and Ag nanoparticles	61
3.8	Characterization techniques	61
3.8.1	Structural Measurements	61

3.8.1.1	X-ray diffraction (XRD)	61
3.8.1.2	Transmission electron microscopy	62
3.8.1.3	Field Emission Scanning Electron Microscopy (FE-SEM)	62
3.8.1.4	Raman spectroscopy	62
3.9	Optical Measurements	63
3.10	Atomic absorption spectroscopy (AAS)	63
3.11	Electrical Measurements	64
3.11.1	Hall Effect	64
3.12	Gas Sensor System	65
<b>Chapter Four: Result and Discussion</b>		
4.1	Introduction	67
4.2	Optical Properties of Au and Ag nanoparticles	67
4.2.1	UV-visible studies	67
4.3	Structural and Morphological Characteristics of Nanoparticles	69
4.3.1	X-ray Diffraction Results	69
4.3.2	TEM studies of Au and Ag nanoparticles	72
4.4	Structural and Morphological Characteristics of ZnO and SnO <sub>2</sub> thin films	80
4.4.1	FE-SEM analysis of ZnO and SnO <sub>2</sub> thin films	80
4.4.2	X-ray Diffraction Results	84
4.4.3	The crystallite size and Lattice parameters	86
4.5	Optical properties of ZnO and SnO <sub>2</sub> thin films	88
4.5.1	Absorbance (A)	88
4.5.2	Absorption Coefficient ( $\alpha$ )	89
4.5.3	Optical Energy gap (E <sub>g</sub> )	91
4.6	Electrical properties	92
4.6.1	Hall Effect	92
4.7	Morphological and Structural Characteristics of ZnO and SnO <sub>2</sub> thin films embedded with Au and Ag	94
4.7.1	FE-SEM analysis for ZnO and SnO <sub>2</sub> embedded with Au and Ag NPs	94
4.7.2	X-ray Diffraction Results for ZnO and SnO <sub>2</sub> embedded with Au and Ag NPs	98
4.8	The crystallite size and Lattice parameters	100
4.9	Raman spectroscopy studies	103
4.10	Optical properties of ZnO and SnO <sub>2</sub> embedded with Au and Ag NPs	106
4.10.1	Absorbance	106
4.10.2	Absorption Coefficient ( $\alpha$ )	109

4.10.3	Optical Energy gap ( $E_g$ )	110
4.11	Electrical properties	112
4.11.1	Hall Effect measurements	112
4.12	Gas Sensor result	114
4.12.1	Influence of the operating temperature of gas sensor	114
4.12.2	Response Time and Recovery Time	116
4.12.3	The Influence of Gas Concentration on Sensitivity	126
4.13	Conclusion	128
4.14	Future Work	130
	References	131

### List of Tables

Table No.	Title	Page No.
1.1	Some properties of $\text{SnO}_2$	5
1.2	Some properties of $\text{ZnO}$	6
1.3	Physical properties of Au and Ag noble metals	9
2.1	Semiconductor materials with current applications and band-gap measurements	30
3.1	Physical and chemical properties of the source materials used to synthesis metal oxides ( $\text{SnO}_2$ and $\text{ZnO}$ ).	55
4.1	The Concentration of gold and silver nanoparticles using atomic absorption spectroscopy	69
4.2	Experimental and standard results of X-ray diffraction of gold nanoparticles.	70
4.3	Experimental and standard results of X-ray diffraction of silver nanoparticles.	71
4.4	The size distributions of gold NPs at different number of pulses (150, 250, 350, 450, 550 and 650) estimated from TEM micrographs(nm)	76
4.5	The size distributions of silver NPs at different number of pulses (150, 250, 350, 450, 550 and 650) estimated from TEM micrographs (nm)	79
4.6	X-ray diffraction results of $\text{ZnO}$ thin films.	87
4.7	X-ray diffraction results of $\text{SnO}_2$ thin films	87
4.8	Hall Effect measurements of $\text{ZnO}$ at different molarities	93
4.9	Hall Effect measurements of $\text{SnO}_2$ at different molarities	93



4.10	Structural parameters for ZnO+Ag at different volume ratios (4:1 and 3:2)	100
4.11	Structural parameters for ZnO+Au at different volume ratios (4:1 and 3:2)	101
4.12	Structural parameters for SnO <sub>2</sub> +Ag at different volume ratios (4:1 and 3:2)	102
4.13	Structural parameters for SnO <sub>2</sub> +Au at different volume ratios (4:1 and 3:2)	102
4.14	Hall Effect measurements of pure ZnO(0.5M) thin films embedded with Au and Ag NPs at different volume ratios (3:2 and 4:1)	113
4.15	Tables(4.15): Hall Effect measurements of pure SnO <sub>2</sub> (0.5M) thin films embedded with Au and Ag NPs at different volume ratios (3:2 and 4:1)	113

### List of Figures

No.	Title	Page No.
1.1	Classification of thin film deposition techniques	2
1.2	The lattice tetragonal rutile structure of SnO <sub>2</sub>	4
1.3	ZnO crystal structures: cubic zinc blende and hexagonal (wurtzite)	6
1.4	Different methods for the synthesis of nanoparticles	10
1.5	Schematic illustrating key elements of the PLA process	12
1.6	A schematic diagram of the experimental setup of laser ablation	13
1.7	Steps for preparation of thin films and powders by the sol gel process	16
2.1	The optical transitions (a) Allowed direct, (b) Forbidden direct (c) Allowed indirect, (d) Forbidden indirect	33
2.2	Schematic diagram of UV-Visible spectrophotometer	35
2.3	The absorption edge and the main absorption regions	36
2.4	Schematically illustrates interference between wave scattering from two adjacent rows of atoms in a crystal	38
2.5	Estimation the crystallite size by (W-H) method	39
2.6	Geometry of the Hall effect experimental	44
2.7	Schematic diagram of band bending after chemisorptions of charged species. $\Lambda_{air}$ : thickness of the space-charge layer, eV surface potential barrier.	47
2.8	Schematic responses curve of (MOS) gas sensor	49

3.1	The main steps of the experimental work	54
3.2	preparation procedure of ZnO and SnO <sub>2</sub> thin films	57
3.3	(A) Spin coating system , (B) A schematic diagram of Spin coating	58
3.4	Photograph image for laser ablation system	59
3.5	Color of gold (Au) and silver (Ag) nanoparticles colloidal solutions using different numbers of pulses	60
3.6	Schematic diagram of the thin film deposition experimental	60
3.7	Block diagram of UV–Visible spectrometer	63
3.8	A block diagram of Atomic absorption spectroscopy.	63
3.9	Electrical circuit diagram used to measure the Hall Effect	64
3.10	Gas sensor testing system	65
3.11	Schematic diagram of gas sensing and the electrical circuit setup	66
4.1	UV–Vis absorption spectra of gold NPs synthesized by PLAL technique using different numbers of pulses (150, 250, 350, 450, 550 and 650)	68
4.2	UV–Vis absorption spectra of silver NPs synthesized by PLAL technique using different numbers of pulses (150, 250, 350, 450, 550 and 650)	68
4.3	X-ray diffraction patterns of gold nanoparticles at different number of pulses (150, 250, 350, 450, 550 and 650)	70
4.4	X-ray diffraction patterns of silver nanoparticles at different number of pulses (150, 250, 350, 450, 550 and 650)	72
4.5	TEM micrograph images and corresponding size distributions of gold NPs at 150 pulses	73
4.6	TEM micrograph images and corresponding size distributions of gold NPs at 250 pulses	73
4.7	TEM micrograph images and corresponding size distributions of gold NPs at 350 pulses	74
4.8	TEM micrograph images and corresponding size distributions of gold NPs at 450 pulses	74
4.9	TEM micrograph images and corresponding size distributions of gold NPs at 550 pulses	75
4.10	TEM micrograph images and corresponding size distributions of gold NPs at 650 pulses	75
4.11	TEM micrograph images and corresponding size distributions of Silver NPs at 150 pulses	76

4.12	TEM micrograph images and corresponding size distributions of Silver NPs at 250 pulses	77
4.13	TEM micrograph images and corresponding size distributions of Silver NPs at 350 Pulses	77
4.14	TEM micrograph images and corresponding size distributions of Silver NPs at 450 pulses	78
4.15	TEM micrograph images and corresponding size distributions of Silver NPs at 550 pulses	78
4.16	TEM micrograph images and corresponding size distributions of Silver NPs at 650 pulses	79
4.17	FE-SEM images of ZnO thin films for (0.3 M) at two magnifications (50 kx and 100 kx)	81
4.18	FE-SEM images of ZnO thin films for (0.5 M) at two magnifications (30 kx and 100 kx)	81
4.19	FE-SEM images of ZnO thin films for (0.7 M) at two magnifications (50 kx and 100 kx)	82
4.20	FE-SEM images of SnO <sub>2</sub> thin films for (0.1M) at two magnifications (100 KX and 150 KX)	83
4.21	FE-SEM images of SnO <sub>2</sub> thin films for (0.3M) at two magnifications (100 KX and 150 KX)	83
4.22	FE-SEM images of SnO <sub>2</sub> thin films for (0.5M) at two magnifications (100 KX and 150 KX)	84
4.23	XRD patterns of ZnO thin films with various molarities	85
4.24	XRD patterns of SnO <sub>2</sub> thin films with various molarities	86
4.25	Absorbance spectra of ZnO thin films at different molarities	88
4.26	Absorbance spectra of SnO <sub>2</sub> thin films at different molarities	89
4.27	The absorption coefficient as a function of the photon energy of (a) ZnO (b) SnO <sub>2</sub>	90
4.28	The optical energy gap ( $E_g$ ) of the ZnO thin films at different molarities	91
4.29	The optical energy gap ( $E_g$ ) of SnO <sub>2</sub> thin films at different molarities	92
4.30	FE-SEM analysis for ZnO embedding with Au NPs (A) ZnO+Au(3:2)(B) ZnO+Au(4:1) (C,D) Cross – section image	94
4.31	FE-SEM analysis for ZnO embedded with Ag NPs(A) ZnO+Ag(3:2)(B) ZnO+Ag(4:1) (C,D) Cross –section image	95
4.32	FE-SEM analysis for pure SnO <sub>2</sub> embedded with Au NPs (A) SnO <sub>2</sub> +Au(3:2)(B) SnO <sub>2</sub> +Au(4:1) (C,D) Cross – section image	96

4.33	FE-SEM analysis for pure SnO <sub>2</sub> embedded with Ag NPs (A) SnO <sub>2</sub> +Ag(3:2) (B) SnO <sub>2</sub> +Ag(4:1) (C,D) Cross – section image	97
4.34	XRD patterns of ZnO thin films embedded with Au and Ag NPs	98
4.35	XRD patterns of SnO <sub>2</sub> thin films embedded with Au and Ag NPs	99
4.36	Raman spectrum of (a) pure ZnO (b) ZnO+Au(3:2)(c) ZnO+Ag(3:2)	104
4.37	Raman spectrum of (a) pure SnO <sub>2</sub> (b)SnO <sub>2</sub> +Au(3:2) (c) SnO <sub>2</sub> +Ag(3:2)	105
4.38	Absorbance spectra of pure ZnO (0.5M) thin films embedded with Au NPs at different volume ratios (3:2 and 4:1)	106
4.39	Absorbance spectra of pure ZnO (0.5M) thin films embedded with Ag NPs at different volume ratios (3:2 and 4:1)	107
4.40	Absorbance spectra of pure SnO <sub>2</sub> (0.5M) thin films embedded with Au NPs at different volume ratios (3:2 and 4:1)	108
4.41	Absorbance spectra of pure SnO <sub>2</sub> (0.5M) thin films embedded with Ag NPs at different volume ratios (3:2 and 4:1)	108
4.42	The absorption coefficient as a function of the photon energy for ZnO thin films embedded with Au, Ag NPs at different volume ratios (3:2 and 4:1)	109
4.43	The absorption coefficient as a function of the photon energy for SnO <sub>2</sub> thin films embedded with Au, Ag NPs at different volume ratios (3:2 and 4:1)	110
4.44	Optical energy gap of ZnO thin films embedded with Au and Ag NPs at different volume ratios (3:2 and 4:1)	111
4.45	Optical energy gap of SnO <sub>2</sub> thin films embedded with Au and Ag NPs at different volume ratios (3:2 and 4:1)	111
4.46	The variation of sensitivity with the operation temperature of the prepared SnO <sub>2</sub> , ZnO, SnO <sub>2</sub> +Au(3:2),SnO <sub>2</sub> +Ag(3:2), ZnO +Au(3:2), and ZnO+Ag(3:2) to NH <sub>3</sub> gas	115
4.47	The variation of sensitivity with the operation temperature of the prepared SnO <sub>2</sub> , ZnO, SnO <sub>2</sub> +Au(3:2), SnO <sub>2</sub> +Ag(3:2), ZnO +Au(3:2), and ZnO+Ag(3:2) to NO <sub>2</sub> gas	116

4.48	The variation of response time and recovery time with operation temperature of the prepared SnO <sub>2</sub> , ZnO, SnO <sub>2</sub> +Au(3:2), SnO <sub>2</sub> +Ag(3:2), ZnO +Au(3:2) and ZnO+Ag(3:2) gas sensor	118
4.49	The variation resistance with time for different operation temperature of NO <sub>2</sub> and NH <sub>3</sub> gases for the pure SnO <sub>2</sub> gas sensor	120
4.50	The variation resistance with time for different operation temperature of NO <sub>2</sub> and NH <sub>3</sub> gases for the pure ZnO gas sensor	121
4.51	The variation resistance with time for different operation temperature of NO <sub>2</sub> and NH <sub>3</sub> gases for the SnO <sub>2</sub> + Au(3:2) gas sensor	122
4.52	The variation resistance with time for different operation temperature of NO <sub>2</sub> and NH <sub>3</sub> gases for the SnO <sub>2</sub> + Ag(3:2) gas sensor	123
4.53	The variation resistance with time for different operation temperature of NO <sub>2</sub> and NH <sub>3</sub> gases for the ZnO + Au(3:2) gas sensor	124
4.54	The variation resistance with time for different operation temperature of NO <sub>2</sub> and NH <sub>3</sub> gases for the ZnO + Ag(3:2) gas sensor	125
4.55	The variation resistance with time for (200 <sup>0</sup> C) operation temperature of (a) NO <sub>2</sub> and (b) NH <sub>3</sub> gases for ZnO+Au (3:2)	127

## List of Symbols

Symbol	Meaning	Unit
Å	Angstrom	
$\theta$	Diffraction Angle	Degree
$h\nu$	Photon Energy	eV
t	Thickness	nm
$\alpha$	Absorption Coefficient	cm <sup>-1</sup>
a, b, c	Lattice Constants	Å
hkl	Miller Indices	
D <sub>av</sub>	Crystallite size	nm
d <sub>hkl</sub>	Interplanner Spacing	Å
$\beta$	full width at half maximum	Rad
M, M <sub>wt</sub>	M the molar concentration, M <sub>wt</sub> the molecular weight of the material	Mol (g/mol)
N	Number of crystallites per unit area	cm <sup>-2</sup>
$\delta$	Dislocation Density	cm <sup>-2</sup>
S	Micro Strain	%
I <sub>o</sub>	incident light intensity	mW/cm <sup>2</sup>
I	penetrating light intensity	mW/cm <sup>2</sup>
E <sub>g</sub>	Energy gap	eV
E <sub>v</sub>	Valence band energy	eV
E <sub>c</sub>	Conduction band energy	eV
$\lambda$	Wavelength of incident light	nm
h	Planck's constant	J.s
$n^*$	Refractive index	-
T	Transmittance	-
A	Absorbance	-
R	Reflectance	-

A and B	Constants depending on properties of bands	-
$\nu$	Frequency	$s^{-1}$
T	The Absolute Temperature	k
$B_z$	Magnetic Field	Tesla
$\mu_H$	Hall mobility	$m^2 / (V.s)$
$R_H$	Hall coefficient	$m^3/C$
$V_H$	The Hall Voltage	Volt
n	The Carrier Concentration	$Cm^{-3}$
p	The Hole Concentration	$Cm^{-3}$
$\sigma$	Conductivity	$(\Omega.m)^{-1}$
$\rho$	resistivity	$(\Omega.m)$
$\sigma_0$	minimum electrical conductivity at 0 K	$(\Omega.m)^{-1}$
e	The Electron Charge	C
S	Sensitivity	
Ra & Rg	Ra the resistance in air and R <sub>g</sub> is the resistance in presence of test gas	$\Omega$
ppm	parts per million	mg/L

## List of Abbreviations

<b>Abbreviation</b>	<b>Description</b>
UV-Vis	Ultra Violet Visible
IR	Infrared
XRD	X- Ray Diffraction
FESEM	Field Emission Scanning Electron Microscopy
TEM	Transmission Electron Microscopy
SEM	Scanning Electron Microscope.
EDS	Energy Dispersive X-ray spectroscopy
D.C	Direct Current
MOS	Metal Oxide Semiconductor
NPs	Nanoparticles
C.B	Conduction Band
V.B	Valance Band
W-H	Williamson-Hall
SRO	Short Range Order
LRO	Long Range Order
SPR	Surface Plasmon Resonance
Nd:YAG	neodymium doped yttrium aluminum garnet
PLAL	Pulsed Laser Ablation in Liquid
PLA	Pulsed Laser Ablation
SAED	Selected Area Electron Diffraction
AAS	Atomic Absorption Spectroscopy
CVD	Chemical Vapor Deposition
LED	Light-Emitting Diode



LDs	Laser Diodes
APCVD	Atmospheric Pressure Chemical Vapor Deposition
VOC	Volatile Organic Compound
XPS	X-ray Photoelectron Spectroscopy
AES	Auger Electron Spectroscopy

# **Chapter One**

**Introduction**

**and**

**Previous Studies**

## 1.1 Introduction

The term "thin films" refers to a layer or layers of atoms having a thickness of less than  $1\mu\text{m}$  (1000 nm). One of the most recent technologies to be fully determined is the thin film technology. Importantly, it advances research on semiconductors and metals by clearly indicating their chemical and physical properties. Thin films' characteristics typically differ from those of the bulk due to their two-dimensional nature [1]. In bulk, forces acting in all directions are in charge of the particles. In contrast, these forces have an impact on the particles that are on the surface of thin films. Depending on the nature of the research area or other practical applications, the film layer is deposited on specific substrates such as glass slides, silicon wafers, aluminum, and quartz. Currently, thin films have many electronic and optical applications. The electronic applications of thin films have steadily increased over the past decades. This can be due to their wide uses in manufacture of electrical resistors, capacitances, transistors, integrated circuits for digital computers and other electronic devices. In addition, thin films are particularly important in a wide range of optical industries such as development of ordinary and thermal mirrors, high-reflectance mirrors, and semi-transparent reflectance coatings which is used in optical equipments (e.g. filters in solar cells and non-absorbent materials used in interference) [2].

## 1.2 Thin Films Deposition Techniques

As seen in Figure 1.1 [3] the approaches for the deposition of thin films can be split into two main primary categories: physical and chemical techniques.

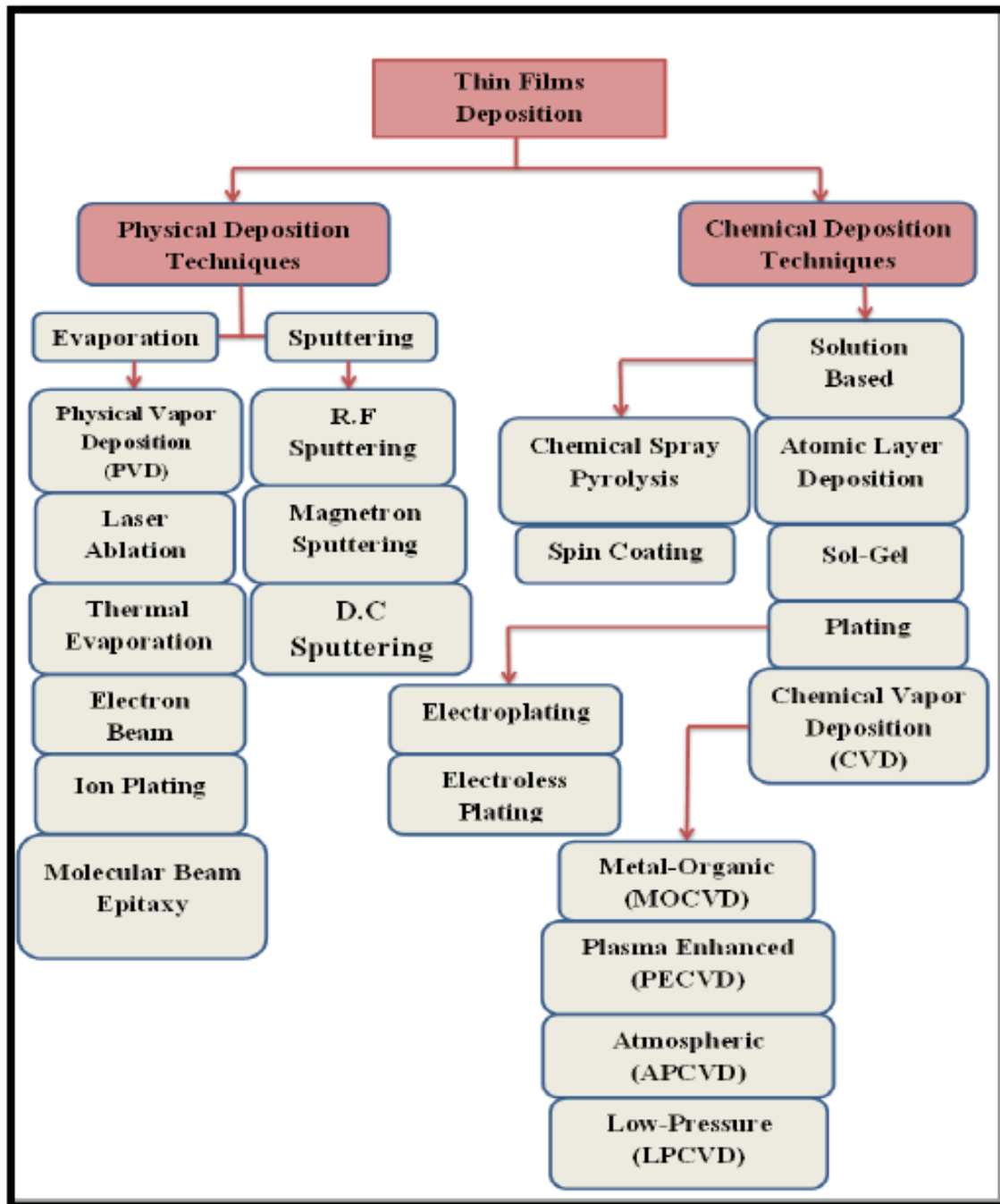


Figure (1.1): Classification of thin film deposition techniques [3]

### 1.3 Metal oxides

Compounds made up of metal atoms and oxygen are called metal oxides. Most metals exist as native metal oxide deposit in nature. Aluminum oxide, for example, accounts for 8.1 have percent of earth's crust. The use and application of thin metal oxide films has been known for a long time, but the demand is still growing. Metal oxides are really prevalent because

electronegative oxygen atoms and the metal have created stable chemical interactions.

Metal oxides are used as capacitors, transistors, computer memory, and other components in semiconducting materials, especially in the microelectronics industry. In order to increase durability and create coatings for energy-efficient glass installations with low emissivity, metal oxide thin films are frequently employed as practical glass coatings [4]. The production and characterisation of thin films with particular ( $\text{SnO}_2$  and  $\text{ZnO}$ ) nanostructures have been produced for gas sensing [5].

Metal oxide gas sensor is made up to interact with a certain group of gases, where they go through an oxidation or reduction process. This technique causes the target gas to exchange an electron with the metal oxide sensors at a specific characteristic rate. This will affect the resistance of the sensor and producing a specific signal. The gas sensor devices provide a range of different features, like small design, low cost, ease of production, simplicity of measurement, and reliability. The theory of metal oxide sensor activity is based on the change in oxide conductivity due to gas contact which is usually proportional to the gas concentration [5,6]. Two kinds of metal oxide sensors are commonly available; n-type (zinc oxide, tin dioxide, iron ( $\text{Fe}_3\text{O}_2$ ) oxide) or titanium dioxide, responding to gas reduction and p-type (nickel oxide, cobalt oxide) reacting to oxidizing gases [7].

Transparent Conducting Oxides (TCOs) are metal oxides with high optical transmittance and high electrical conductivity. They are also referred to as wide-band gap oxide semiconductors.

### 1.3.1 Tin oxide ( $\text{SnO}_2$ )

Tin oxide exhibits a tetragonal rutile structure can be seen when its lattice parameters of  $a=b = 4.737$  and  $c = 3.826 \text{ \AA}$ , and  $\alpha = \beta = \gamma = 90^\circ$ . The unit cell has two tin atoms and four oxygen atoms. Six oxygen atoms are joined to each tin atom in the corners of a regular octahedron. At the corners

three tin atoms of an equilateral triangle surround each oxygen atom [8], as shown in Figure (1.2).

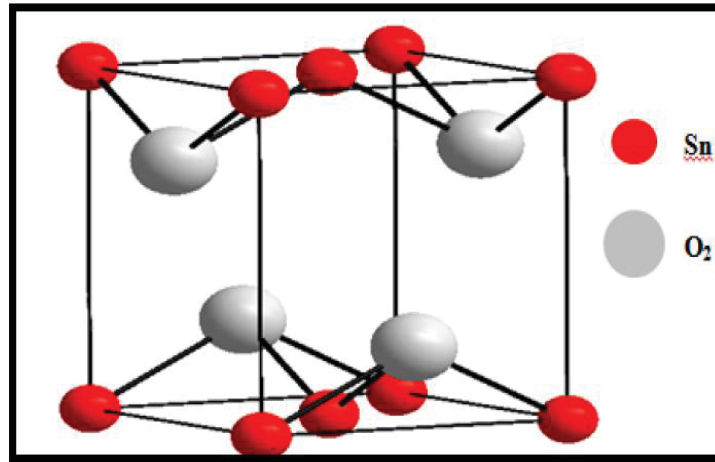


Figure. (1.2): The lattice tetragonal rutile structure of  $\text{SnO}_2$  [8].

The tin chemistry consists of the metal's oxidation number with oxidation states of +2 or +4. These oxidation states are controlled by tin (II) oxide, commonly known as stannous oxide, and tin (IV) oxide, also known as stannic oxide. Sn (II) and Sn (IV) in a variety of oxidation states make up the transitional phases  $\text{Sn}_2\text{O}_3$  and  $\text{Sn}_3\text{O}_4$  [9]. Due to their distinct structural and electrical characteristics, SnO and  $\text{SnO}_2$  have a variety of applications [10]. Tin oxide ( $\text{SnO}_2$ ) films are n-type semiconductors with a wide band gap in the range of (3.6 and 4.3 eV).  $\text{SnO}_2$  semiconducting transparent thin films have a number of attractive properties for technical applications in "solar energy conversion, flat screen displays, electrochromic devices, invisible security circuits, LEDs and gas sensors", etc. As a result, the creation of large area  $\text{SnO}_2$  films on effective and cheap accessible substrates is of great interest.  $\text{SnO}_2$  is a basis in sensors for flammable gases, such as carbon monoxide detectors. In this instance, the sensor surface is heated to a constant temperature, and when a flammable gas is detected, the electrical resistance decreases. [11]. Table (1.1) shows some properties of  $\text{SnO}_2$ .

Table 1.1: some properties of SnO<sub>2</sub> [8].

Properties	Values
Molar Mass	150.71 g/mol
Appearance	White or light grey powder
Density	6.86 g/cm <sup>3</sup>
Melting point	1630 <sup>0</sup> C
Band gap	(3.6- 4.0) eV , direct
Magnetic susceptibility ( $\chi$ )	4.1 x 10 <sup>-5</sup> cm <sup>3</sup> /mol
Refractive index at wavelength 550 nm	2.006

### 1.3.2 Zinc oxide (ZnO)

Zinc oxide (ZnO) has been studied for several decades as an effective semiconductor. One of the most interesting sensor materials is ZnO, which combines unique optical and electrical characteristics. ZnO is a unique substance with a variety of piezoelectric, pyroelectric, and semiconducting properties. ZnO crystal structures: zinc blende and hexagonal (wurtzite). Has some advantages, it is an n-type semiconductor with a direct wide band gap (3.3 eV) and a strong excitation binding energy (60 meV) [12]. It is an essential functional oxide, displaying high conductivity and near ultraviolet emission. Also, ZnO demonstrates a piezoelectric effect, a key feature in the construction of electromechanical-coupled sensors and transducers. ZnO is a water-insoluble white powder and commonly used as an ingredient in many materials and products, glass, cement, lubricants, paints, ointments, adhesives, sealants, pigments, foods and batteries, ferrites, fire retardants, and first aid tapes, materials, rubbers, plastics, ceramics and high-technical applications such as surface acoustic wave filters, photonic crystals, photodetectors, light emitting diodes, photodiodes, optical modulator waveguides, solar cells, varistors, and laser diodes (LDs) provide a broad range of ZnO nanostructures. The advantages of this semiconductor nanostructure included high band gap, clear luminescence at ambient temperature, high electron

mobility, and excellent clarity. [13,14]. Figure (1.3) shows the ZnO crystal structure [14], and table 1.2 depicts some properties of ZnO [15].

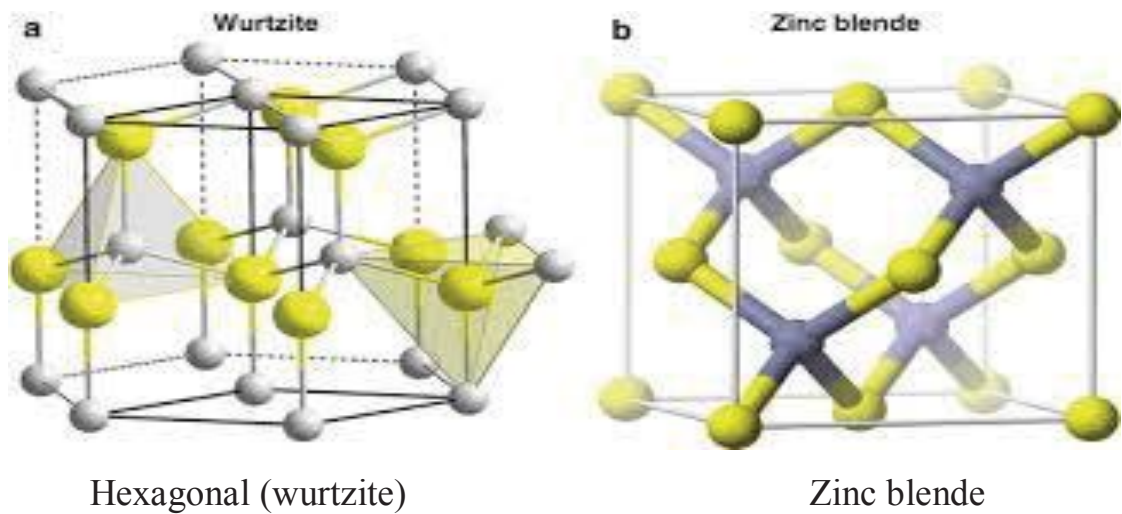


Figure (1.3): ZnO crystal structures: Zinc blende and Hexagonal(wurtzite)[14].

Table 1.2: Some properties of ZnO [15]

Chemical formula	ZnO
Molar mass	81.406 g/mol
Appearance	White solid
Density	5.61 g/cm <sup>3</sup>
Melting point	1975 °C
Band gap	(3.2- 3.4) eV, direct
Magnetic susceptibility ( $\chi$ )	$-27.2 \cdot 10^{-6} \text{ cm}^3/\text{mol}$
Refractive index	2.029



## 1.4 Nanotechnology

The word 'Nanotechnology' was used and characterized early in 1974 by Taniguchi [16]. In addition, the US National Nanotechnology Initiative (NNI) in 2000 as provided by the concept of nanoscience and nanotechnology [17]. The word “*Nano*” refers to  $10^{-9}$  meter is used to describe the materials smaller than the molecules, clusters of atoms or particles in the quantum world [18]. The word "colloid" is more elusive and can vary from nanometers to several hundred micrometers in particle size. Since about the beginning of humanity, people have been attracted by the vibrant colours of noble metals like gold or silver. Additionally, to being applied as a medical substance to treat arthritis, they have been used to colour glass and textiles. Devices that can be used in a variety of physical processes are made using Au colloidal (e.g. surface-enhanced Raman spectroscopy, solar cells, sensors, optoelectronic devices); biological (e.g. drug delivery systems); and biomedical (e.g. diabetic healing, Photothermal therapy, biochemical sensors) applications [19- 28].

## 1.5 Nanoparticles Synthesis Methods

### 1.5.1 Top-down method

The top-down approach usually includes laser ablation, starting from bulk. Basically, This method involves separating a system into its constituent elements. In order to get smaller parts, this method also uses cutting, milling or drilling equipment. It can be used to classify micro-patterning processes including photolithography, plasma etching, and laser ablation. Top down approaches are suffering from the need to reduce huge quantities of material [30].

### **1.5.2 Bottom-up method**

Smaller elements are combined into larger structures using the bottom-up process. To obtain biotechnological elements, single molecules are combined using the bottom-up method. The self-assembly of atoms and molecules is a term used in nanotechnology to describe how larger structures are produced. This form includes the sol-gel method as well as chemical vapor deposition (CVD). [30].

## **1.6 Definition of Nanoparticles**

The word nanoparticle refers to a small particle that ranges between 1 to 100 nanometres in size in three dimensions, made up of a very small number of atoms or molecules, It take a variety of shapes, including spherical, triangular, cubical, pentagonal, rod-shaped, shell-shaped, ellipsoidal, etc.etc. [18]. Due to their high surface area and high degree of electronic conductivity properties, nanoparticles have unusual chemical and physical properties compared to their heavy bulk materials [31]. According to their chemical, physical and biological properties, the metallic nanoparticles are major subjects of research in modern materials science. Noble metal nanoparticles of silver and gold are of particular interest [32].

### **1.6.1 Noble Metal Nanoparticles**

Noble metal such as silver and gold NPs have attracted a great attention because of the special electrical, optical, physical, chemical, and magnetic properties [33]. In the green and red regions of the UV-visible spectrum, both Au and Ag NPs have a plasmonic effect due to the dispersion and absorption of photons. They have stable chemical, physical and biological properties, such as resistance to high temperatures, photo-irradiation, high resistance to oxidation or acids, and catalytic action and properties of biocompatibility. Ag NPs have been used extensively as nanoscale sensors, catalyze, optical data storage anti-bacterial agents in the health industry, food

storage, textile coatings and a number of environmental applications. Furthermore, it could be potentially used as biological labels and electroluminescent displays [34].

Au NPs have many different applications depending on the size of particles. For example, in immune histochemistry, microscopy (light and high magnification TEM) and biomarkers, the small sizes of Au NPs (2 nm-15 nm) are used. In environmental detection and purification, drug distribution, biomarkers, chemical sensors and DNA detection, medium size Au NPs (20-60 nm) are used. Large Au NPs (80 - 250 nm) are used in forensic science, computer devices, optical mammography, manufacturing, etc. [34]. Ag and Au nanoparticles are chemically stable and often display surface enhanced Raman scattering in the visible wavelength range, where they can greatly enhance various optical cross-sections. Table 1.3: show the physical properties of Au and Ag noble metals.

Table 1.3: physical properties of Au and Ag noble metals.

property	Gold	Silver
symbol	Au	Ag
Atomic Number	79	47
Atomic Mass (U)	196.97	107.87
Melting Point(°C)	1064.18	961.8
Boiling Point(°C)	2970	2162
Density g/cm <sup>3</sup>	19.32	10.50
Electrical Conductivity (10 <sup>6</sup> Ω <sup>-1</sup> .m <sup>-1</sup> )	0.442	0.630
Thermal Conductivity (W.m <sup>-1</sup> .k <sup>-1</sup> )	318	429
Refractive Index	0.20	0.135

### 1.6.2 Nanoparticles preparation techniques

There are many techniques that can be used to prepare nanoparticles, including as photo-reduction, flame metal combustion, electrochemical reduction, solvothermal electrolysis, chemical fluid deposition, and spray pyrolysis. Metal salts are often reduced chemically in the presence of enabling

molecules to produce noble metal nanoparticles. Additionally, the top-down generation of NPs is now frequently done by pulsed laser ablation in liquid (PLAL). The relatively new PLAL technique was initially presented in 1993 by "Fojtik" et al. [35]. It has attracted attention as a top-down methodology of operation. Different processes have been used to synthesize nanoparticles of silver and gold. Nanoparticles have been produced by biological, physical, and chemical processes. Figure (1.4) show the different methods for the synthesis of nanoparticles [36].

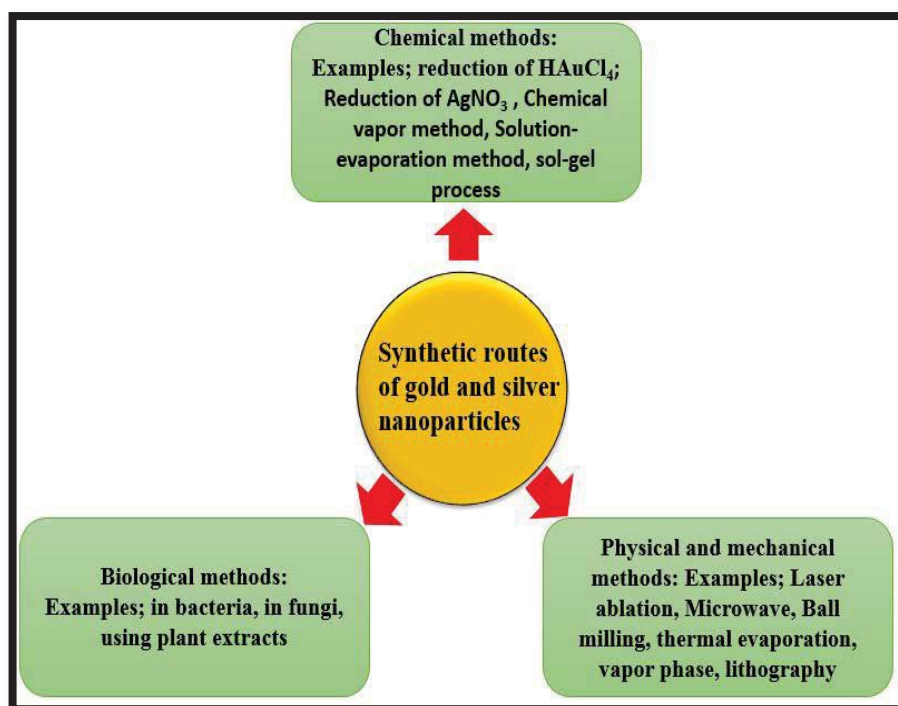


Figure (1.4): Different methods for the synthesis of nanoparticles [36].

## 1.7 Pulsed Laser Ablation (PLA) Method

Pulsed laser can be used to vaporize the plume of material that tightly restricted of both temporally and spatially, this method can be used instead of simply evaporating material for the production of vapor supersaturated [36]. Laser ablation is convenient method to generate nanoparticles from the gas phase [37]. In other words, PLA method can only fabricate little quantities of

nanoparticles. PLA technique can control the size distribution and maintain the purity of the crystal such as Si nanoparticles [38]. PLA method can be used to vaporize materials that are difficult to evaporate by other methods [36].

Basically, in pulsed laser ablation process, the beam of pulsed laser is focused onto target (target in solid phase), then the target is partially evaporating with each laser pulse [37]. The target is usually rotated with each new pulse of laser because the rate of material removal by laser ablation decreases with longer target exposure time [39]. Laser such as Nd:YAG with wavelength (1064 nm and/or 532 nm) is usually used as a pulsed laser source in the PLA process [36]. When the surface of target is hit or shot by laser beam, the interaction happened between the surface of target and laser beam. Surface of the target is heated much higher than the boiling point of target material to be in the vapor phase. This vapor becomes superheated and ionized leading to form a plasma phase. Carrier gas (inert gas) flowing on the heated surface target cools the vapor and carries nanoparticles away from the area of laser ablation [37]. Schematic examples of main elements of the pulsed laser ablation mechanism are shown in Figure (1.5), where (a) depicts the initial laser radiation absorption (depicted by long arrows), the start of melting and vaporization (shaded area indicates melted material, short arrows indicate motion at the solid-liquid interface), and (b) illustrates how the melt front spreads into the solid, continuing vaporization, and becoming important by the start of laser-plume interaction., (c) suggests the absorption by the plume of incident laser radiation and the production of plasma, and finally (d) indicates that the front of the melt recedes, contributing to subsequent re-solidification [40].

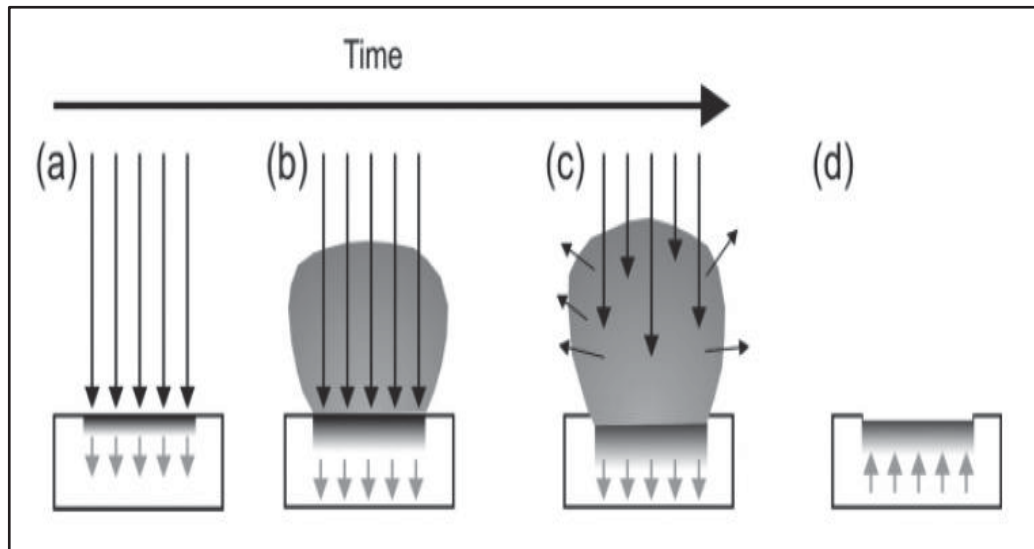


Figure (1.5): Schematic illustrating key elements of the PLA process [40].

Now the beam of a pulsed laser onto a target material under low pressure or vacuum, it should be noted of background gas or in liquid such as water or ethanol solutions [40]. The following list of elements, which can influence and regulate particle size, can be used to describe them. [41]

- a) The Laser parameters: fluence, wavelength and pulse duration parameters.
- b) The ambient gas conditions: type of liquid pressure, nature and flow parameters.

### 1.7.1 Pulse Laser Ablation in Liquids (PLAL)

A promising top-down method for managing the production of nanomaterials is pulsed laser ablation in liquid media (PLAL), where ablated molecules are rapidly responsively quenched at the plasma-liquid interface. Noble metals, alloys, oxides, and semiconductors can all be deposited using the easy PLAL technique. It can create nanoparticles without counter-ions or surface-active materials, making it simple and without constraints. A metal target is exposed to a high-power pulsed laser beam that creates a local plasma with a high temperature (about 6000 K) and high pressure at the solid-liquid interface [42-44].

The Pulse Laser Ablation in Liquid method has many advantages, such as:

- 1- Simple and easy experimental setup.
- 2- Low cost because it does not always need a vacuum chamber.
- 3- Environmentally friendly because no toxic or dangerous gases are released.
- 4- We are able to make pure NPs colloid devoid from impurities [45].
- 5- This technique can use a variety of liquids and targets and is quick.
- 6- NPs can be produced without the need for heat treatment because the confinement effect causes the temperature and pressure of the plasma created by the pulse laser to be much higher than those of a vacuum or a gas on the target surface immersed in liquid. Figure (1.6) shows a schematic diagram of the experimental setup of laser ablation for synthesis nanoparticles from solid target immersed in aqueous solution. A lens is often used to focus the Nd-YAG laser beam onto a metallic target. The target is fixed by a holder at the bottom of a quartz container [46].

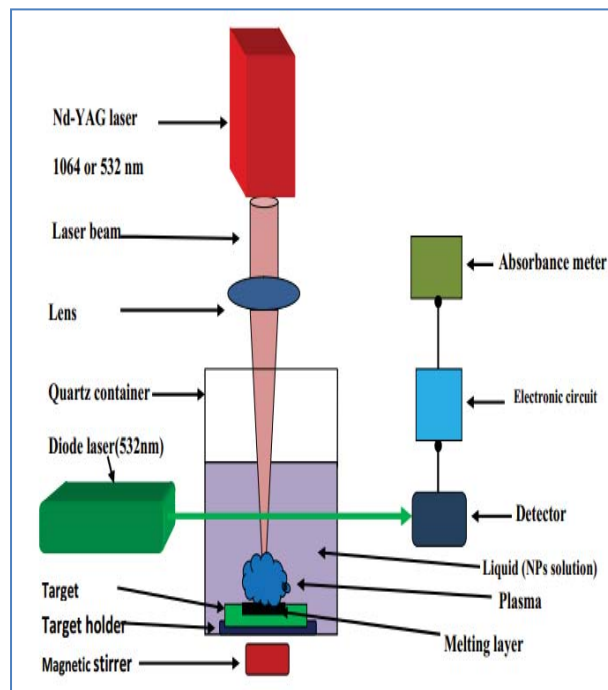


Figure (1.6): A schematic diagram of the experimental setup of laser ablation [46].

## 1.8 Spin coating technique

Spin coating method is an essential technique used in development and deposition of organic and inorganic thin films [47]. Films that produced by this method are highly reproducible and homogenous. During spin coating process, two forces are acting on the solution; the adhesive forces at the solution substrate interface and the centrifugal forces resulting from the high-speed rotation. These competing forces will cause a strong shearing action at the interface which could lead to form a thin film with adjustable thickness depending on the angular velocity, solution concentration and the viscosity. There are several critical factors in homogeneous films production, such as solvent evaporation rate, fluid viscosity, solution concentration, angular velocity (rotating velocity) and spinning time [48]. The liquid is first placed onto the substrate in the "spin coating process", and then the substrate is accelerated to the spinning speed that was designed for it. A minute quantity of film is absorbed by the substrate as a result of the motion caused by centrifugal force [49]. The effect of gravity force on the spin coating can be traditionally ignored, as the formation of thin film under spinning dominates the substrate adsorption.

speed in spin coating is one of the most essential factors. The speed of the substrate affects the radial (centrifugal) force applied to the liquid as well as the speed and usual turbulence of the air immediately above it [50]. The force imparted to the fluid solution as it approaches the substrate's edge must be balanced with the rate of drying, which impacts viscosity, to determine the film thickness. Additionally, the substrate's acceleration toward the maximum spin speed may have an effect on the properties of the coated film. Acceleration must be precisely controlled since the solution starts to dry during the early portion of the spin cycle. The coat characteristics of patterned substrates are also significantly influenced by acceleration [51].



## 1.9 The sol-gel method

sol-gel techniques combine a variety of techniques for creating materials from solutions, and one of its processing steps involves the formation of gel, sol-gel is a chemical techniques that are used to form colloidal oxides either from chemical solution or from colloidal particles of nanostructure. The most prevalent kind of sol-gel synthesis relies on controlled chemical hydrolysis [52]. The polycondensation and hydrolysis process that occurs during the first stage of this process result in the synthesis of an initial colloidal solution, also referred to as a sol of hydroxide particles with a size in the nano range. The applications of sol-gel process are many. One example is the use of metal-organic or inorganic material as precursors in sol-gel method to create thin film coatings [53].

Centrifugal of gravitational exhaustion is used to create thin films, which determines the form of the fluid outline, the magnitude of the forces acting on the solid phase, and the time of the deposition process. This is followed by continuous stirring and drying. This method allows to get of the materials at low temperatures. It is an ideal technique for preparing thin films, nanotubes, powders and fibers. Figure (1.7) represent Sol gel process steps for synthesizing thin films and powders [54,55].

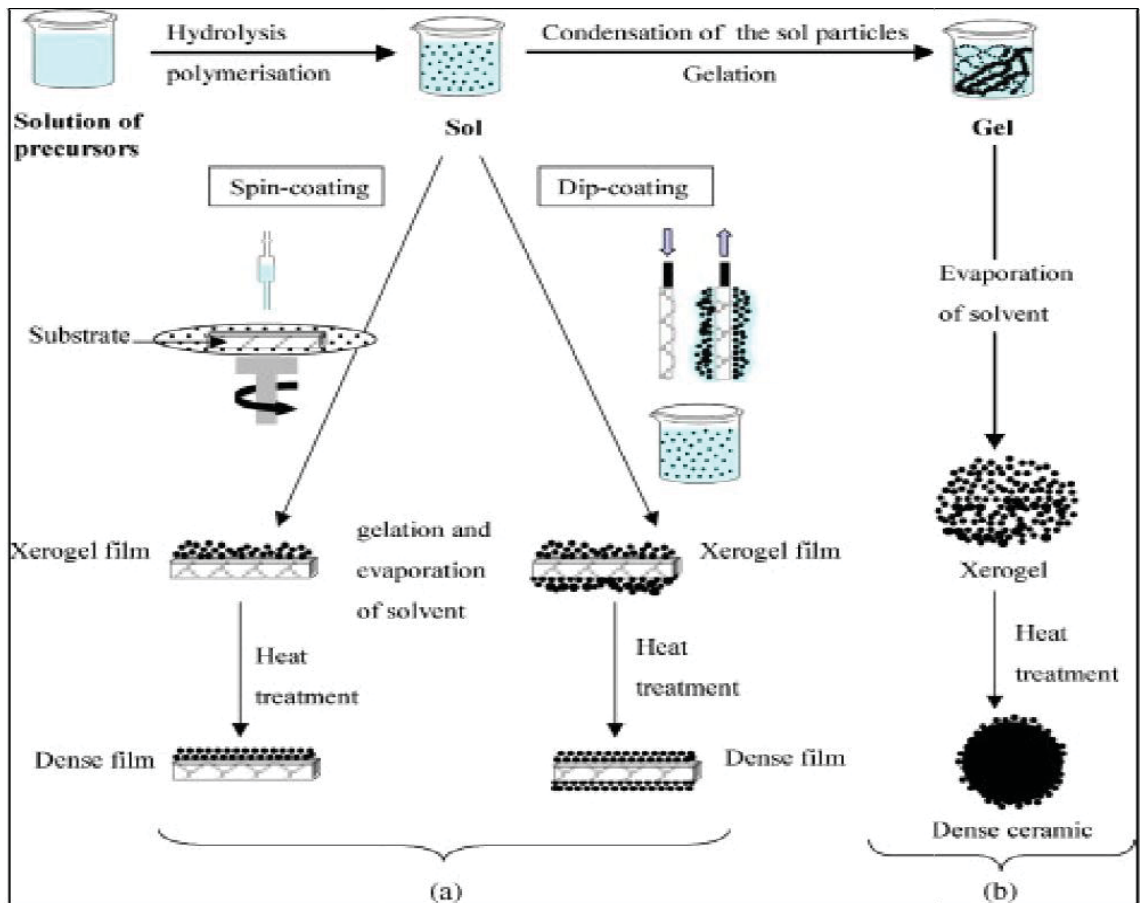


Figure (1.7): Steps for preparation of thin films and powders by the sol gel process [54].

## 1.10 Previous Studies

In 2010, Gupta et al. developed a variety of ZnO nanostructures, such as nanowires and nanobelts, to prepare thick films (with variable grain boundaries) and isolated nanowire/nanobelt gas sensors. Sensors for H<sub>2</sub>S and NO gases were tested for their sensitivity. They found that both intragrain resistances and grain boundaries get a factor in the NO gas reaction, grain boundaries alone are responsible for the response of ZnO sensors to H<sub>2</sub>S gas. Additionally, they discovered that the sensors built using isolated nanobelts responded to NO with a very specific set of characteristics [56].

In 2010, Ahpark et al. manufactured SnO<sub>2</sub>-ZnO hybrid nanofibers by using the pulsed laser deposition and electro spinning techniques. After calcination

at 600 °C, SnO nanocrystalline coated ZnO nanofibers with a random network topology were produced. SnO<sub>2</sub> deposit had a fiber diameter of 55–80 nm and a size of 10-15 nm, respectively. At a temperature of 200°C, the sensor that was composed of SnO<sub>2</sub>-ZnO hybrid nanofibers demonstrated a very strong gas response to concentrations of NO<sub>2</sub> as low as 400 parts per billion [57].

In 2010, Qunxiang et al. synthesized Ag nanoparticles embedded-ZnO nanorods by photochemical method. TEM, XPS, DSC, XRD, and SEM were used to characterize the samples after they were prepared. The characterization results showed that ZnO nanorods included Ag nanoparticles that had been enclosed within them. Additionally, the properties of Ag NPs inserted in ZnO nanorods for gas sensing were studied. The response of Ag NPs embedded-ZnO nanorod sensors to 50 ppm ethanol was almost identical to that of sensors made from pure-ZnO nanorods, given the possibility of improving the efficiency of the sensors by including Ag NPs into the surfaces of ZnO nanorods. It was discovered that the Ag NPs embedded-ZnO nanorod sensors had good stability and significantly improved gas-sensing performances in their response and selectivity for detecting ethanol vapor. [58].

In 2012, Enrico et al. fabricated 40–50 nm thickness of NiO and ZnO thin films with inserted Au nanoparticles by the sol–gel technique. The films made of nanocomposites are crystalline and porous, and the optical absorption in the visible range depends on the concentration of gold nanoparticles. These films were studied as a possible optical and electrical sensor for the detection of polluting gases. It has been determined that H<sub>2</sub>, CO, and NO<sub>2</sub> all have a rapid response. The optical characteristics is considering the sensing of both NiO and ZnO films over the gold surface plasmon resonance peak

wavelength spectrum have been found to be enhanced by gold nanoparticles. Additionally, the optical response of ZnO was improved by the presence of Au, even though Au NPs are optically inactive in this range. In addition, It was shown that the reducing gases inject electrons into the oxide, and that Au nanoparticles immediately detect the charge variation by combining the observed shift in the surface plasmon resonance peak with the different semiconductive types of the two oxides [59].

In 2012, Vural synthesized a wide variety of NPs by PLAL, including magnetic nanostructures, semiconductors, nanoalloys, noble metals, base metals, and core-shell nanostructures. It was reported that PLAL could synthesize Au, Ag, and Pt NPs in a variety of liquid environments using a Nd: YLF laser ( Q-Switched Laser, 527 nm wavelength, 16 W average power, 110 ns pulse duration, and 16 mJ pulse energy for 1 kHz ). First, nanoparticles of silver, gold, and platinum have been produced in deionized water using a pulsed Nd: YLF laser. Second, similar conditions were used to manufacture these NPs in methanol. After that, transmission electron microscopy, scanning electron microscopy, X-ray photoelectron spectroscopy, X-ray diffractometer, and UV-Vis Photospectrometer analysis techniques were used to characterize the colloidal NP solutions. A UV-Vis photospectrometer and transmission electron microscopy were used to analyze the Au and Ag NPs after they had been incorporated in nanofibrous composites [60].

In 2013, Niranjana and Gupta developed ethanol sensor using hydrothermally produced zinc oxide (ZnO) nanowires modified with a thin layer of Au (~10 nm). At an operating temperature of 325 °C, the sensor films respond most effectively to the presence of ethanol. The response and recovery times for Au modified sensor films towards 50 ppm of ethanol at 325 °C were 5 and

20 s, respectively. The addition of Au not only improved the reaction kinetics toward ethanol but also improved the sensor response. This improved sensing performance according to the electronic sensitization process and the nano-Schottky barriers type connection between Au and ZnO were the causes of the faster reaction kinetics [61].

In 2013, Machmudah et al. produced silver and gold nanoparticles used PLA in pressured CO<sub>2</sub>. Under different pressures, 532 nm laser ablation was utilized as the excitation wavelength. The variations in CO<sub>2</sub> density and the lengthening of the ablation duration both had a substantial impact on the architectures of Au and Ag nanoparticles. A network structure of smaller gold particles was created, as evidenced by a field-emission scanning electron microscopy (FE-SEM) image of the gold nano-structured particles on silicon wafer. The following could be seen as the nanoparticle production process: During the ablation process, the larger gold/silver particles were melted, and the smaller, spherical nanoparticles that were expelled from them formed nanoclusters were connected to the molten particles [62].

In 2015, Rajesh et al. used ZnO nanoparticles to establish NO<sub>2</sub> gas sensors. A variety of ZnO nanomaterials, including thin films, nanosheets, quantum dots, nanorods, nanowires, and nano-micro flowers, were employed in the fabrication of NO<sub>2</sub> gas sensors. The fundamental characteristics of gas sensors, including recovery time, reaction time, selectivity, limit detection, gas response, stability, and recyclability, etc. were explored. The effects of several variables on the NO<sub>2</sub> gas sensing characteristics, including the concentrations of NO<sub>2</sub>, the annealing temperature (T), the morphologies and particle sizes of ZnO, the relative humidity, and the operating temperatures, were also discussed [63].

In 2015, Tharsika employed a single-step thermal evaporation process with carbon assisted to make ZnO and SnO<sub>2</sub> nanostructures with various morphologies, and investigated into their gas sensing capabilities. Tin oxide, zinc oxide, and carbon powders made up the source material, which was combined and placed into a quartz boat before even being put in the center of a tube furnace. Nanostructures were studied using (XRD), (FESEM), (TEM), and (EDS) to determine their crystallographic phase, microstructure, and elemental composition. In the hierarchical nanostructures, ZnO branches took on a hexagonal shape as they developed on the ZnO shell layer. With short response and recovery durations, The sensitivity and selectivity of Zn<sub>2</sub>SnO<sub>4</sub> nanowire-based sensors for ethanol were excellent. Ethanol concentrations as low as 20 ppm can be detected by SnO<sub>2</sub> core/ZnO shell hierarchical nanostructures at 400 °C was five times greater than that of pure SnO<sub>2</sub> nanowires after 90 minutes of deposition. Highly active sensing was suggested to be responsible for this increase in ethanol sensitivity [64].

In 2016, Li et al. manufactured modified ZnO (Au/ZnO) NPs using a "bamboo cellulose template and the calcination" method. They studied the gas-sensing capabilities of Au/ZnO NPs -based sensors. Comparing the Au/ZnO NPs to pure ZnO, the results showed an improvement in gas sensing performance. The Au/ZnO NPs responded about 2.7 times more effectively to 100 ppm ethanol (50) at 240 °C than they did to acetone., indicating a stronger selectivity for ethanol. This high reaction to ethanol may be caused by the small size, Schottky barrier, and catalysis [65].

In 2016, Aled et al. developed a simple chemical process that allowed them to create highly sensitive gold nanoparticle coated (decorated) zinc oxide nanosheet gas sensors. These sensors were able to provide a normalized current gain of 2.54 (at 10V) in dry air that contained 2.5ppm of hydrogen gas

while being heated to 200 degrees Celsius. Gold nanoparticles having a mean diameter of 5 nm were used in a straightforward "microwave-assisted hydrothermal" growth approach to bring up the formation of zinc oxide nanosheets. At a temperature of 200 degrees Celsius, a response of 1.24 was obtained for concentrations of ppm less than 125 when compared to sensors based on undecorated sheets [66].

In 2017, Borhaninla et al. created varying concentrations of gold nanoparticles combined with tin dioxide nanoparticles in the laboratory, and then studied the CO sensing characteristics of the resulting compounds. For the preparation of the first solution, the sol-gel method was utilized. For the purpose of characterizing the nanoparticles, XRD, SEM, TEM, DLS, and spectrophotometry were utilized. At an operational temperature of 340 degrees Celsius, the pure sensors exhibited a response of approximately 4 to 12.8 for  $(20-80 \text{ s}) \times 10^{-6} \text{ CO}$ . At a concentration of  $50 \times 10^{-6} \text{ CO}$ , the reaction time is approximately 10 seconds, and the recovery time is around 14 seconds [67].

In 2017, Sonik et al. The production of zinc oxide (ZnO) nanoparticles was carried out by using a combination of two distinct processes: thermal evaporation in a two-zone furnace and simple heat treatment. As a film that was deposited on glass substrate, Zn acetate dihydrate at concentration of 0.17 M was used for both of these processes. The XRD, FESEM, FTIR, and UV-Vis spectrophotometers, as well as the LCR meter, were utilized in order to characterize the ZnO that was synthesized. The results of the XRD analysis showed that the wurtzite crystals had a hexagonal structure with a preferential orientation along the (101) plane. According to the findings of FESEM, the grain size was in the region of 50 to 5 nm. After looking into the optical properties, researchers came to the conclusion that the band gap can be found

in the range of 3.32–3.36 eV. At an operating temperature of 250 degrees Celsius, the gas sensing properties demonstrated a higher response in the case of thermal evaporation in comparison to a typical heat treatment [68].

In 2017, Roberto et al. created an ether gas-sensor and also relies on gold nanoparticles (Au NPs) that are coated zinc oxide microstructures. Measurements taken using a "scanning electron microscope (SEM) and a high-resolution transmission electron microscope (HRTEM) were used to investigate the structural and morphological properties. In a relatively low temperature range, the response of gas sensing was studied, with a range that between 150 and 250 °C . When compared to a sensor that was made from pure ZnO. The sensor's ether gas response was noticeably better at the highest possible working temperature when it was constructed on Au NPs coated ZnO. In point of fact, a sensor entirely built on ZnO demonstrated only a rather low sensitivity of roughly 25 percent [69].

In 2017, Sachin et al. Utilizing tin oxide ( $\text{SnO}_2$ ) thin film by a conventional spin coating sol-gel process with  $\text{SnCl}_4 \cdot 2\text{H}_2\text{O}$  as a precursor. XRD, SEM, TEM, FTIR, PL, and UV-Vis" techniques were used to examine the film's optical, electrical, structural, and gas sensing characteristics. The samples had a tetragonal rutile structure, according to XRD and Transmission Electron Microscopy, which revealed that the average particle size was approximately (11.26)nm. At various operating temperatures and concentrations, ethanol gas sensing of manufactured  $\text{SnO}_2$  thin film was evaluated [70].

In 2018, Gisane et al. synthesized ZnO nanorod-Au nanoparticle hybrids on a substrate. In order to be utilised in gas sensor devices, ZnO nanorods were grown on  $\text{Al}_2\text{O}_3$  substrates at low temperatures by chemical bath deposition. A sputtering process was then used to deposit Au NPs. The studies from



SEM, XRD, EDX and TEM indicated that the Au NPs uniformly covered the ZnO nanorods surface and that the hexagon-based ZnO nanorods grew perpendicularly to one another on the substrate. When compared to ZnO nanorods at 300 °C, the ZnO-Au NPs hybrid-based sensor showed an enhanced sensor response for H<sub>2</sub> and O<sub>2</sub> gases [71].

In 2018, Shano prepared PANi NFs and copper nanostructures [ CuO and tin oxide (SnO<sub>2</sub>)] used the hydrothermal process and spin coating at room temperature to deposit PANi NFs, CuO, SnO<sub>2</sub>, and their composites on glass and silicon substrates with a thickness of nearly 325 nm. For inorganic - polyaniline films, the surface morphological, optical, structural, electrical, photoconductivity, and gas sensing properties have been investigated. The XRD results revealed that the PANi films are naturally crystalline, and that the composites of PANi/SnO<sub>2</sub> and SnO<sub>2</sub> nanostructures are polycrystalline and have tetragonal structures. The sensitivity to H<sub>2</sub>S gas was increased with the increase in the operating temperatures and SnO<sub>2</sub> and CuO concentration. The highest H<sub>2</sub>S gas sensitivity to nanocomposites PANi/CuO films was obtained at high CuO concentrations and was determined to be 260 % at (T<sub>o</sub>= 200 °C) . The recovery times and response increased as operating temperature increased, showing a quick response time (0.753 s) and recovery time (0.787 s) at (30°C)[72].

In 2018, Ganesh et al. Ag/ZnO composite nanostructures with high sensitivity ammonia gas sensor were used, and their optical, morphological, structural, and gas sensing characteristics were investigated. STEM examination clearly showed that the Ag/ZnO composite had a flower-like shape. Ag, Zn, and O were evenly distributed, according to STEM-mapping measurements. According to the ammonia gas sensing analysis, the Ag/ZnO (6 wt%) showed

a greater gas response than other Ag wt% contents. The maximum response was 29.5 when Ag/ZnO (6 wt%) was treated to 100 ppm ammonia gas [73].

In 2019, Saleh synthesized ZnO and SnO<sub>2</sub> nanostructures thin films on glass substrate by hydrothermal drop casting techniques and atmospheric pressure chemical vapor deposition. Tin chloride, zinc acetate, zinc nitrate and hexamethylenetetramine (HMTA), were used in this process. The atmospheric pressure chemical vapor deposition (APCVD) system was used to obtain the optimized thin films by taking appropriate deposition conditions, such as substrate temperature, flow rate of gas, quality and location of deposition within the system reactor. The morphology, structural, surface roughness and optical properties were studied by (XRD), (FE-SEM), (EDS), (AFM), UV-Vis spectroscopy, respectively and gas sensing properties have been investigated for (SnO<sub>2</sub> and ZnO) thin films. X-ray diffraction (XRD) analysis was performed for all samples prepared at different substrate temperatures (300, 400, 450, 500, 550 and 600°C) and different oxygen gas flow rates (4, 5, 6, and 8 NL/h). It was observed that by increasing the oxygen flow rates and substrate temperatures, the crystallite size increased [74].

In 2019, Chen et al. by using a one-pot hydrothermal process, ZnO nanowires/Au NPs and ZnO nanowires hybrid (Au-ZNWs) with different concentrations of Au were produced and examined by SEM, XRD, XPS, TEM, and FTIR. Structure-characterisation results showed that Au nanoparticles had self-assembled on the surface of ZNWs. According to gas sensing properties, 1 mol % Au-ZNWs had the best sensing results when compared to pure ZNWs and Au-ZNWs" with various Au concentrations. At 150 °C. The greatest response of 1 mol% Au-ZNWs to 1 ppm NO<sub>2</sub> was 31.4, which was more than 4 times the 8.2 of pure ZNWs. Compared to pure ZNWs, Au-ZNWs with different concentrations of Au exhibited higher selectivity to NO<sub>2</sub> [75].

In 2019, Mohamedkhair et al. fabricated silver nanoparticles with Tin oxide films as H<sub>2</sub> gas sensors. Various characterization techniques, such as UV-Vis absorption, X-ray photoelectron spectroscopy, XRD, FESEM, and AFM, were used to characterize thin films for composition, structural, and morphological properties. X-ray photoelectron spectroscopy analysis revealed the presence of silver/silver oxide on SnO<sub>2</sub> thin films. At various hydrogen gas concentrations, the gas sensing characteristics of the produced sensors were examined. It was discovered that the manufactured sensor in greater concentrations (beginning at 600 ppm) can be detected even at room temperature [76].

In 2019, Wu et al. based High-sensitive ammonia sensors on self-assembling SnO nanoshells were made by employing a solution method and annealing at 300 °C for an hour. The as-fabricated sensors displayed responses of 313%, 874%, 2757%, 3116%, and 3757% ( $\Delta G/G$ ) for ammonia concentrations of (5, 20, 50, 100, and 200 parts per billion), respectively. The structure of the nanoshells, which includes curved shells that protect the core and a large surface area, allowed them to absorb more ammonia molecules, increasing the sensitivity much farther. Additionally, the SnO nanoshells showed improvement than other metal oxide ammonia sensing materials because they had larger oxygen vacancy concentrations [77].

In 2019, Beniwal et al. used Sol-gel spin coating technology to prepare SnO<sub>2</sub> nanostructured thin film-based gas sensor. The sensor was tested for the concentration range of 500 ppb–500 ppm for ammonia (NH<sub>3</sub>) solution, acetone (C<sub>3</sub>H<sub>6</sub>O), methanol (CH<sub>3</sub>OH), and 2-propanol (C<sub>3</sub>H<sub>8</sub>O) at room temperature (RT) with humidity level 55 % RH. With a very fast response and recovery time at RT, high response and good selectivity towards ammonia were found. The porous nanograins-based SnO<sub>2</sub> thin film layer, with an average particle size of 50 nm, was credited for the sensor's high response

at RT. Other characteristics of the manufactured device were high accuracy and a sizable resilience to drift behavior. The produced SnO<sub>2</sub> thin film's structural, chemical composition, topography, and morphological properties were examined using the results of X-Ray diffraction (XRD), X-Ray Photoelectron Spectroscopy (XPS), Atomic Force Microscopy (AFM), and Scanning Electron Microscopy (SEM) , respectively. The ammonia gas sensors produced from Sample response by (313, 874, 2757, 3116, and 3757 %) , respectively, for gas concentrations of 5 ppm, 20 ppm, 50 ppm, 100 ppm, and 200 ppm [78].

In 2020, Wang et al. synthesized Zinc oxide (ZnO) nanoparticles with dispersed silver (Ag) nanoparticles (Ag-ZnO) by calcining electrospun nanofiber precursors. Ag to Zn ratios of 0, 1, 3, and 5% were found in the precursor solutions. Sensor microstructure was studied using SEM and TEM. XRD and X-ray photoelectron spectroscopy revealed the presence of metallic Ag, and the characteristics of gas sensing of Ag-ZnO were studied. After mixing ZnO nanoparticles with Ag nanoparticles, the gas sensing efficiency of ethanol and hydrogen sulfide was excellent (H<sub>2</sub>S). The response/recovery times of the 3 % of Ag-ZnO sensor to ethanol were only 5 and 9 s, respectively. However, H<sub>2</sub>S exhibited a high response value in all of the Ag-ZnO-based gas sensors [79].

In 2020, Mehrabi et al. developed a volatile organic compound (VOCs) using a metal oxide semiconductor (MOS) sensor, which are essential for noninvasive diagnostics or the control of dangerous chemicals. Electrospinning was used to create the sensor from tin dioxide (SnO<sub>2</sub>) and poly (ethylene oxide). Sputtering was used to achieve the gold doping of the composite nanofibers and a high-temperature oven was used for the calcination process. To establish the best fabrication parameters that produce great sensitivity, the activity of the sensor with various calcination temperatures and doping thicknesses was examined. The perfect gold dopant

thickness was discovered to be 10 nm, However, the optimal temperature and time for calcination were determined to be 350 °C and 4 hours, respectively. [80].

In 2021, Petrov et al. developed a novel solid-phase low-temperature pyrolysis process to create thin nanocomposite films of ZnO and SnO<sub>2</sub> at concentrations of 0.5 to 5% mol%. To compare with electrical and gas-sensing properties, this hetero-oxide material was fully investigated using (XRD), (SEM), X-ray photoelectron spectroscopy (XPS), and Auger electron spectroscopy (AES) techniques. They discovered that the films are composed of ZnO and SnO<sub>2</sub> crystals with average grain sizes in the region of 10-15 nm. The specimen whose Sn:Zn optimum ratio was determined to be 1:99 demonstrates a 1.5-fold improvement when exposed to 5-50 parts per billion NO<sub>2</sub> at 200 degrees Celsius. while testing the chemical resistance of the films with various concentrations of tin dioxide. These remarkable changes have developed at this rational composite by reducing the intergrain potential barrier to 0.58 eV and raising the concentration of anionic vacancies. The results indicate that solid-phase low-temperature pyrolysis is an useful technique for modifying the oxide ratio components to modify the functional gas-sensing properties of hetero-oxide films [81].

In 2022 , Tahani et al prepared ZnO thin film and a silver-doped zinc oxide nanocomposite Ag/ZnO thin film by the technique of the pulsed laser deposition at 600 °C to be applicable as a portable catalytic material for the removal of 4-nitrophenol. The nanocomposites was prepared by making the deposition of the two targets (Zn and Ag), and it was analyzed by different techniques. According to the XRD pattern, the hexagonal wurtzite crystalline form of Ag-doped ZnO NPs suggested that the samples were polycrystalline. Additionally, the shifting of the diffraction peaks to the higher angles, which denotes that doping reduces the crystallite size. From SEM images, Ag-doping drastically altered the morphological characteristics and reduced the

aggregation. Additionally, its energy band gap decreased when Ag was incorporated. UV spectroscopy was then used to monitor the catalysis process. According to the catalytic experiment results, the Ag/ZnO thin film has remarkable potential for use in environmentally-favorable applications.[82]

### **1.11 Aims of the Work**

- 1) Study of the characteristics of (Au and Ag) nanoparticles prepared by using pulsed laser ablation in liquid (PLAL).
- 2) Study of the characteristics of (SnO<sub>2</sub> and ZnO) nanostructure thin films using a sol-gel spin coating technique.
- 3) Optimizing the conditions for preparation of Au and Ag nanoparticles embedded ZnO and SnO<sub>2</sub> thin films regarding their structural, electrical and optical properties.
- 4) Enhancement of gas sensor properties by embedded ZnO and SnO<sub>2</sub> thin films with Au and Ag NPs towards NH<sub>3</sub> and NO<sub>2</sub> gasses with high quality performance (response time, recovery time, sensitivity and stability).